Acta Biomaterialia xxx (xxxx) xxx



Contents lists available at ScienceDirect

Acta Biomaterialia

journal homepage: www.elsevier.com/locate/actbio



Full length article

Non-enzymatic glycation increases the failure risk of annulus fibrosus by predisposing the extrafibrillar matrix to greater stresses

Minhao Zhou^{a,1}, Erin S. Archibeck^{a,1}, Yarah Feteih^a, Yousuf Abubakr^a, Grace D. O'Connell^{b,c,*}

- ^a Department of Mechanical Engineering, University of California, Berkeley, 2162 Etcheverry Hall, #1740, Berkeley, CA 94720-1740, USA
- ^b Department of Mechanical Engineering, University of California, Berkeley, 5122 Etcheverry Hall, #1740, Berkeley, CA 94720-1740, USA
- ^c Department of Orthopaedic Surgery, University of California, San Francisco, San Francisco, USA

ARTICLE INFO

Article history: Received 15 March 2023 Revised 13 June 2023 Accepted 6 July 2023 Available online xxx

Keywords:
Intervertebral disc
Annulus fibrosus
Advanced glycation end-products
Diabetes
Tissue failure

ABSTRACT

Growing clinical evidence suggests a correlation between diabetes and more frequent and severe intervertebral disc failure, partially attributed to accelerated advanced glycation end-products (AGE) accumulation in the annulus fibrosus (AF) through non-enzymatic glycation. However, in vitro glycation (i.e., crosslinking) reportedly improved AF uniaxial tensile mechanical properties, contradicting clinical observations. Thus, this study used a combined experimental-computational approach to evaluate the effect of AGEs on anisotropic AF tensile mechanics, applying finite element models (FEMs) to complement experimental testing and examine difficult-to-measure subtissue-level mechanics. Methylglyoxal-based treatments were applied to induce three physiologically relevant AGE levels in vitro. Models incorporated crosslinks by adapting our previously validated structure-based FEM framework. Experimental results showed that a threefold increase in AGE content resulted in a \sim 55% increase in AF circumferential-radial tensile modulus and failure stress and a 40% increase in radial failure stress. Failure strain was unaffected by non-enzymatic glycation. Adapted FEMs accurately predicted experimental AF mechanics with glycation. Model predictions showed that glycation increased stresses in the extrafibrillar matrix under physiologic deformations, which may increase tissue mechanical failure or trigger catabolic remodeling, providing insight into the relationship between AGE accumulation and increased tissue failure. Our findings also added to the existing literature regarding crosslinking structures, indicating that AGEs had a greater effect along the fiber direction, while interlamellar radial crosslinks were improbable in the AF. In summary, the combined approach presented a powerful tool for examining multiscale structure-function relationships with disease progression in fiber-reinforced soft tissues, which is essential for developing effective therapeutic measures.

Statement of significance

Increasing clinical evidence correlates diabetes with premature intervertebral disc failure, likely due to advanced glycation end-products (AGE) accumulation in the annulus fibrosus (AF). However, *in vitro* glycation reportedly increases AF tensile stiffness and toughness, contradicting clinical observations. Using a combined experimental-computational approach, our work shows that increases in AF bulk tensile mechanical properties with glycation are achieved at the risk of exposing the extrafibrillar matrix to increased stresses under physiologic deformations, which may increase tissue mechanical failure or trigger catabolic remodeling. Computational results indicate that crosslinks along the fiber direction account for 90% of the increased tissue stiffness with glycation, adding to the existing literature. These findings provide insight into the multiscale structure-function relationship between AGE accumulation and tissue failure.

© 2023 Published by Elsevier Ltd on behalf of Acta Materialia Inc.

* Corresponding author at: Department of Mechanical Engineering, University of California, Berkeley, 5122 Etcheverry Hall, #1740, Berkeley, CA 94720-1740, USA.

1. Introduction

Low back pain is a prevalent global health concern affecting 80% of the adult population and is the leading cause of productivity loss, disability, and healthcare expenditures in many regions

https://doi.org/10.1016/j.actbio.2023.07.003

 $1742-7061/\mathbb{O}$ 2023 Published by Elsevier Ltd on behalf of Acta Materialia Inc.

Please cite this article as: M. Zhou, E.S. Archibeck, Y. Feteih et al., Non-enzymatic glycation increases the failure risk of annulus fibrosus by predisposing the extrafibrillar matrix to greater stresses, Acta Biomaterialia, https://doi.org/10.1016/j.actbio.2023.07.003

E-mail address: g.oconnell@berkeley.edu (G.D. O'Connell).

¹ These authors contributed equally to this work.

JID: ACTBIO [m5G; July 13, 2023;16:12]

around the world [1]. The need for improved low back pain management has amplified in recent years, driven by an aging population and the global diabetes epidemic [2–4]. Over the last few decades, there has been a continual increase in global diabetes prevalence, with more than 10% of the world's population being affected [3,4]. Growing clinical evidence has linked diabetes to intervertebral disc degenerative disorders. Particularly, diabetic patients are \sim 50% more likely to be diagnosed with disc degenerative disorders, with a longer duration or poorer control of diabetes correlating with a more severe level of degeneration [5–8]. Diabetes is also a significant risk factor for lumbar disc herniation, reportedly increasing its risk by \sim 50% after correcting for risk factors such as age, body mass index, lifestyle, and disease history [9].

M. Zhou, E.S. Archibeck, Y. Feteih et al.

The intervertebral disc, situated between adjacent vertebrae in the spinal column, is a fibrocartilaginous joint that plays a crucial biomechanical role during daily activities, including supporting multiaxial spinal loads and motions, as well as dissipating energy. The disc is a highly complex, heterogeneous, hierarchical structure comprising a soft gel-like nucleus pulposus center surrounded by a tough, fiber-reinforced annulus fibrosus (AF) ring [10]. Particularly, the AF consists of 15-25 concentric lamellae of angle-ply collagen fibers embedded in a hydrated proteoglycan-rich extracellular matrix, resulting in excellent load-bearing and energy absorption capacities [10]. However, the disc is highly avascular with limited self-healing capabilities; thus, the heavy biomechanical demand placed on the disc makes the AF susceptible to catabolic tissue remodeling with degeneration and disease [11,12]. Such catabolic remodeling has been shown to initiate, aggravate, or predispose the AF and surrounding structures to irreversible mechanical damage (e.g., tears and disruption), causing debilitating low back pain [11,12].

A well-documented diabetes-induced structural remodeling in the AF is the accelerated formation and accumulation of advanced glycation end-products (AGE) via non-enzymatic glycation [13–15]. AGEs are a heterogeneous group of chemical compounds that can form irreversible crosslinks with extracellular proteins [13,15]. The highly collagenous AF is particularly susceptible to AGE modification due to the minimal biological turnover and extended half-life (up to \sim 120 years) of collagen fibers [16,17]. Understanding the AF structure-function relationship with non-enzymatic glycation can provide valuable insight into disc mechanical failure mechanisms in diabetic patients, which is pivotal for developing effective therapeutic interventions for tissue failure prevention.

Previous in vitro studies examining the effect of non-enzymatic crosslinks on AF uniaxial tensile mechanics have reported increased tissue stiffness and energetic toughness along the evaluated loading directions [18,19]. Likewise, our recent work, which was the first to investigate AF uniaxial tensile mechanics at physiologically relevant AGE levels, reported that glycation significantly increased AF tensile modulus, failure stress, and energetic toughness in the circumferential-axial direction (Fig. 1A - 'Circ-ax specimen') [20]. Joint-level disc mechanics evaluations from studies that induced in vitro crosslinking or used diabetic rodent models fed by AGEs-rich diets also reported higher joint stability and stiffness [21–25]. Therefore, while clinical observations report more frequent and severe tissue failure with AGE accumulation, in vitro mechanical testing results suggest improved tissue mechanical properties with non-enzymatic crosslinking, leaving the relationship between AGE accumulation and tissue failure unclear.

The knowledge of crosslinking structures at the subtissue scale remains limited due to experimental constraints, despite considerable efforts to investigate the functional role of AGEs. Previous work has developed a constitutive relationship to describe AF uniaxial tensile mechanics with non-enzymatic glycation. Still, the relationship was limited to the two-dimensional space and one sample orientation [18]. Finite element models

(FEMs) can predict hard-to-measure stress-strain distributions in complex fiber-reinforced tissues. Through combined experimental-FEM study designs, our previous work successfully used FEMs to guide experimental studies and corroborate experimental hypotheses [26,27]. Additionally, we have developed and validated a multiscale structure-based FEM framework for the AF, which is able to investigate multiscale structure-function relationships in healthy and degenerated AF tissues under various loading and boundary conditions [28–31]. This framework also has the potential to be adapted to describe AF mechanics with non-enzymatic glycation.

Acta Biomaterialia xxx (xxxx) xxx

Thus, the current study aimed to examine the effect of AGEs on anisotropic AF uniaxial tensile mechanics through a combined experimental-computational approach. To achieve this, we evaluated the impact of AGEs on AF uniaxial tensile mechanics on formerly unexamined orientations (circumferential-radial and radial directions). We also adapted our previous multiscale structurebased FEM framework to describe AF mechanics with crosslinking. The validated model was applied to examine subtissue-level stress-strain distributions, aiming to provide mechanistic explanations for premature tissue failure observed with AGE accumulation. Compared to past AGE-oriented AF mechanics studies, the current study was the first to use a combined experimental-FEM approach, which allowed assessment of subtissue-level stress-strain distributions that are difficult to determine directly through bulk tissue experimental testing. The validated models provided valuable insight into the effect of AGEs at the subtissue scale, including the likely orientation of crosslinking structures and extrafibrillar matrix stress distributions. We hypothesized that the improved bulk AF mechanical properties with non-enzymatic glycation were achieved at the risk of exposing the extrafibrillar matrix to increased damage accumulation through mechanical failure and catabolic remodeling.

2. Materials and methods

2.1. Experimental testing

2.1.1. Sample preparation

Bovine discs were used due to their improved accessibility and comparable size, mechanical properties, matrix structures, and biochemical composition to human discs [32-35]. Fresh, skeletally mature, healthy bovine caudal spine sections were acquired from a local butcher (age = 18-24 months; n = 10 spines). Musculature around the discs was removed using a scalpel to prepare disc specimens from C2 to C5 (n = 30 discs). AF specimens oriented in the circumferential-radial and radial directions were prepared from the freshly dissected discs (Fig. 1A - 'Circ-rad specimen' and 'Radial specimen'). A freezing stage microtome was used to obtain 2 mm-thick rectangular specimens. A custom-built cutting tool was used to ensure a specimen width of 5 mm, while sample length depended on the specimen orientation, with an average of 10 mm for circumferential-radial and 5 mm for radial samples. Both circumferential-radial and radial specimens contained \sim 10-15 lamellae. To ensure repeatable midlength failure, a 1 mm thick, full-width notch was created using a custom-made cutting jig in the specimen thickness direction for the circumferentialradial samples [26]. Preliminary testing showed that radial specimens exhibited limited grip failure. Thus, the radial specimens were unnotched. Previous studies reported no significant differences in stiffness or strength between notched and intact fiberreinforced soft tissue specimens and demonstrated a limited effect of stress concentrations at the notch site [36].

Circumferential-radial specimens were prepared with one of the following three soaking protocols to obtain physiologically relevant AGE levels *in vitro*. Samples in the control group (CTRL) were soaked for 18 h at 25°C in a solution containing 5% phosphate-

JID: ACTBIO [m5G; July 13, 2023;16:12]

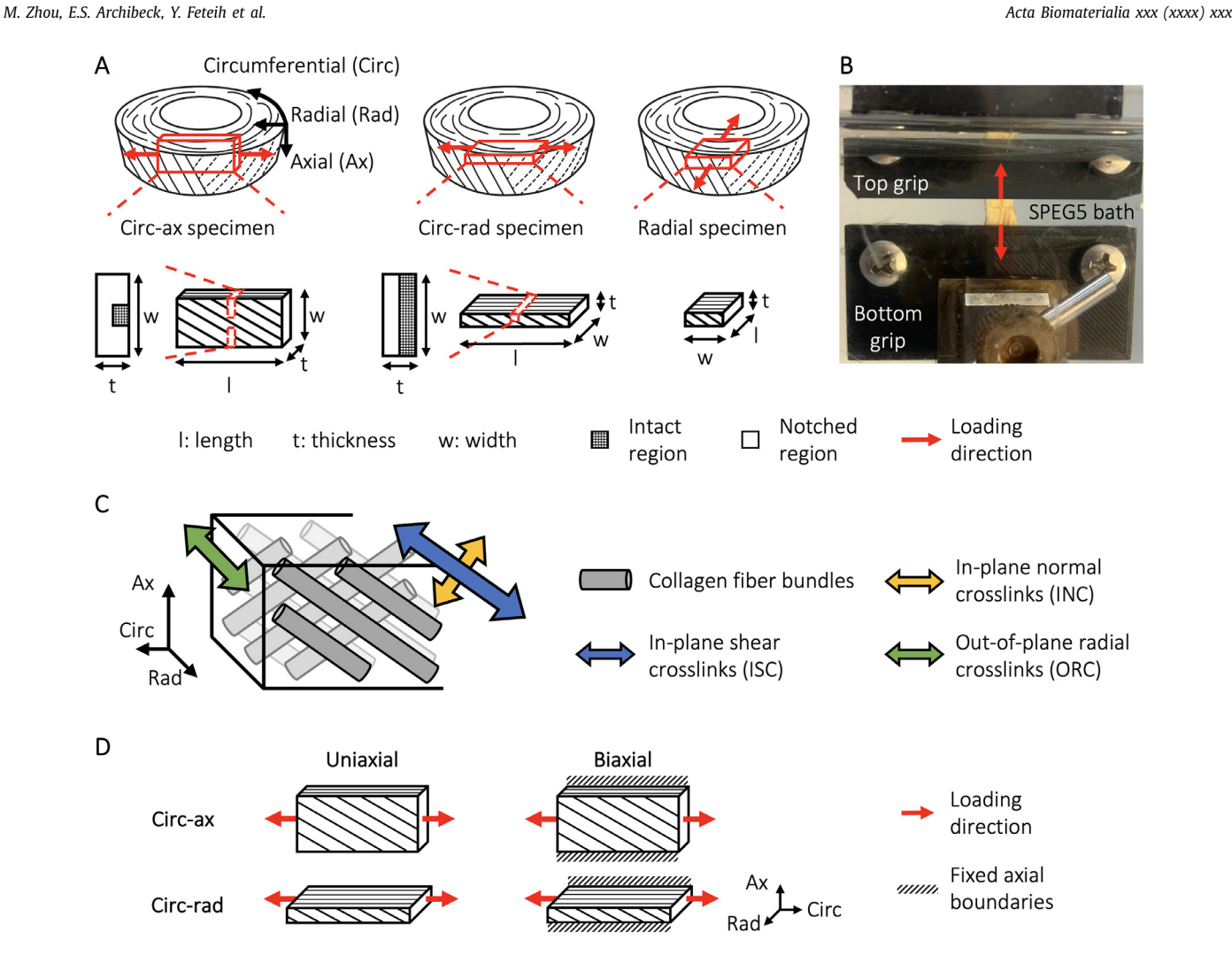


Fig. 1. (A) Schematics of specimen orientation, loading direction (red arrows), and midlength notch geometry for the experimental specimens and validation FEMs. (B) Circumferential-radial sample gripped by the custom-made serrated screw-clamp grips and soaked in an SPEG5 bath during testing. Red arrows represent the loading direction. Model schematics demonstrating (C) possible crosslink orientations and (D) simulated uniaxial and biaxial boundary conditions. The models in (D) were developed to examine multiscale AF mechanics under the uniaxial and biaxial boundary conditions and were created without a midlength notch. (For interpretation of the references to colour in this figure legend, the reader is referred to the web version of this article.)

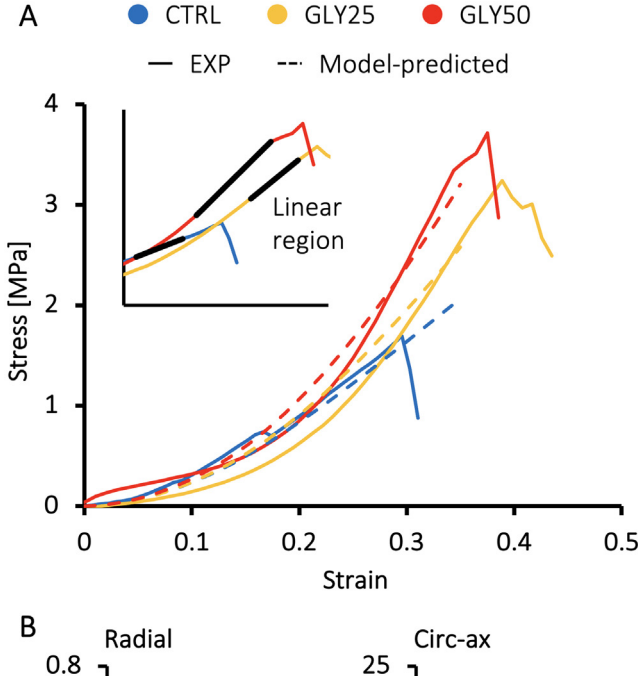
buffer solution and 5%w/v polyethylene glycol (i.e., SPEG5 solution) to minimize excessive tissue swelling [20,27]. Glycated samples were soaked in 0.3 M methylglyoxal at either 25°C (GLY25) or 50°C (GLY50) [20]. All soaking solutions were pH-balanced to 7.4, and previous work showed that incubation at 50°C did not alter bulk AF mechanics or composition [34]. Only CTRL and GLY50 groups were prepared for radial specimens, which had collagen fibers oriented perpendicular to the loading direction, resulting in minimal fiber engagement.

2.1.2. Mechanical testing

Samples were gripped for mechanical testing using a pair of custom-made serrated screw-clamp grips and were placed in a SPEG5 solution water bath to maintain physiologic tissue hydration throughout testing (up to \sim 170 min; Fig. 1B). A monotonic 0.1 N preload was applied to remove slack from the tissue. Scale bar photographs of each specimen were taken to measure the initial sample-specific specimen length (circumferential-radial specimen: 9.64 ± 1.46 mm; radial specimen: 4.94 ± 1.48 mm). Uniaxial tension was applied monotonically along the circumferential direction for the circumferential-radial samples (n = 15 per treatment group) and radial direction for the radial samples (n = 8 per treatment group) at a quasistatic loading rate (0.1 mm/min, 0.017%/sec).

Mechanical testing ended when the specimens were separated into two pieces with no load-bearing capability. Rate-dependent differences were assessed for the circumferential-radial specimens at a high loading rate (50 mm/min, 8.33%/sec, n = 17 per treatment group). Preliminary testing showed that rate-dependent mechanics variations for these specimens followed a similar trend to that reported for the circumferential-axial samples [20]. Since the objective of the current study was to investigate the effect of AGEs on anisotropic AF uniaxial tensile mechanics, high-rate mechanics data are only presented in **Supplementary Fig. 1**. Unless otherwise specified, the remainder of this article presents mechanical testing data obtained at the quasistatic loading rate.

For each specimen that demonstrated a clean midlength failure, engineering stress-strain response was analyzed to facilitate comparison to the existing literature. Engineering stress was calculated as the measured force divided by the initial cross-sectional area evaluated at specimen midlength. Engineering strain was calculated as the tester crosshead displacement divided by the initial gauge (specimen) length. Bulk tensile modulus was calculated at the linear region to ensure physiologic relevance and facilitate comparison with prior literature. The linear region of the circumferential-radial specimen was identified using a custom linear regression optimization algorithm. The algorithm excluded the



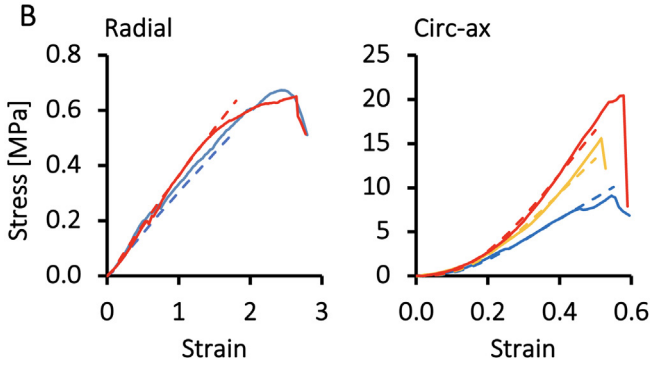


Fig. 2. Representative experimental (EXP) and model-predicted engineering stress-strain curves at each glycation level for **(A)** circumferential-radial and **(B)** radial and circumferential-axial specimens. Data reported for circumferential-axial samples were adapted from Werbner et al. for model validation [20]. Inset in **(A)** demonstrates the linear regions calculated by the custom linear regression optimization algorithm using bolded black line segments.

toe and yield regions of the stress-strain response and calculated the linear region by determining the maximum range within the stress-strain response in which the change in slope remained within a selected threshold (5%) for strain increments of 0.75% (Fig. 2A – inset). Failure stress and strain were recorded at the maximum force during testing. The 'failure energy ratio' was also calculated as the strain energy density up to the point of failure divided by the total strain energy density [20].

2.1.3. Biochemistry

After mechanical testing, a 3 mm biopsy punch was used to extract tissue near the failure sites. Tissue samples were blotted dry using a Kimwipe prior to wet weight measurements. The tissue samples were then lyophilized for 48 h for dry weight measurements. Water content was calculated as the difference between the wet and dry weight divided by the wet weight. Collagen content was measured using the ortho-hydroxyproline (OHP) colorimetric assay, assuming a 1:7.5 OHP-to-collagen mass ratio [37]. Total fluorescence, which estimated the AGE content, was assessed using a quinine sulfate standard at excitation/emission wavelengths of 370 nm/440 nm and was reported as equivalent nanograms of quinine normalized by tissue dry weight [20]. Biochemistry assessments were conducted on the circumferential-radial specimens.

2.1.4. Statistical methods

A priori power analysis was performed using data reported by Werbner et al. to calculate the necessary sample size to achieve a significance level of 0.05 and a power of 0.95 [20]. Pairwise permutation tests with repeated measures were conducted between treatment groups for all mechanical and biochemical properties, as a few datasets did not pass the Shapiro-Wilk Normality Test. All measurements were reported as mean \pm standard deviation since most datasets (> 80%) followed a normal distribution. Bivariate linear correlations were established between tensile modulus and AGE content and between failure stress and AGE content for the circumferential-radial specimens. Correlation strength was determined based on the correlation coefficient R (weak: |R| < 0.5, moderate: $0.50 \le |R| < 0.70$, strong: $|R| \ge 0.70$). A two-way analysis of covariance (ANCOVA) was performed to compare the regression models for the circumferential-radial specimens in this study to the circumferential-axial regression models reported by Werbner et al. (independent variable: AGE content; fixed factor: specimen orientation) [20]. Significance for the permutation tests and ANCOVA was assumed at p < 0.05.

2.2. Finite element modeling

2.2.1. Model development and validation

For this study, we adapted a previously validated multiscale structure-based FEM framework developed for the AF [28]. For brevity, only essential model development details are provided, but the reader is encouraged to refer to the previous paper for additional information. In short, the AF was modeled as a fiberreinforced composite, where the extrafibrillar matrix and collagen fiber bundles were described as distinct materials occupying separate volumes, and the fiber bundles were described as fulllength cylinders uniformly distributed throughout the lamellae and welded to the surrounding matrix (Fig. 1C) [28,38,39]. The geometries and dimensions of the validation FEMs were developed to represent rectangular experimental specimens oriented in the circumferential-axial, circumferential-radial, and radial directions (Fig. 1A) [20]. Individual AF lamellae were modeled as 0.4 mm thick [40], with collagen fibers orienting at $\pm 35^{\circ}$ to the anatomical transverse plane to represent samples prepared from the middleouter AF [41]. Model geometries also included a midlength notch for the circumferential-axial and circumferential-radial specimens (Fig. 1A). Circumferential-axial (~950k elements), circumferentialradial (~850k elements), and radial models (~420k elements) contained five, twelve, and eleven lamellae, respectively, which were consistent with the number of lamellae in experimental specimens. Model material descriptions and boundary and loading conditions were defined in FEBio Studio, and the fully defined FEMs were solved by the FEBio solver [42].

Triphasic mixture theory was applied to describe tissue hydration [43]. Model fixed charge density represented tissue proteoglycan content and was set to -100 mmol/L for the matrix and 0 mmol/L for the fibers [34,44,45]. To describe the AF solid phase, the extrafibrillar matrix was modeled as a Neo-Hookean material [29], where the Young's modulus (0.5 MPa) and Poisson's ratio (0.3) were determined based on *in vitro* AF measurements [46,47]. Collagen fibers were modeled as a compressible hyperelastic ground matrix substance reinforced by a power-linear fiber description to describe AF nonlinearity and anisotropy. The ground matrix substance was modeled using the same Neo-Hookean material described above. For the power-linear fiber description (Eq. (1)), β represented the power-law exponent in the toe region, E_{lin} represented the fiber modulus in the linear region, λ_0 represented the transition stretch between the toe and linear regions, and B was a function of β , E_{lin} , and λ_0 ($B = \frac{E_{lin}}{2} \left(\frac{\lambda_0^2 - 1}{2(\beta - 1)\lambda_0^3} + \frac{1}{\lambda_0} \right)$). Fiber pawars a function of β , E_{lin} , and E_{lin} are regions.

JID: ACTBIO [m5G;July 13, 2023;16:12]

M. Zhou, E.S. Archibeck, Y. Feteih et al.

Acta Biomaterialia xxx (xxxx) xxx

rameters ($E_{\text{lin}} = 60$ MPa, $\beta = 4$, and $\lambda_0 = 1.09$) were determined based on our previously validated models and reported AF fiber bundle mechanical testing data [28,48].

$$\begin{split} & \psi_{n} \big(\lambda_{n} \big) \\ & = \begin{cases} 0 & \lambda_{n} < 1 \\ \frac{E_{\text{lin}}}{4\beta \left(\beta - 1 \right) \lambda_{0}^{3}} \left(\lambda_{0}^{2} - 1 \right)^{2 - \beta} \left(\lambda_{n} - 1 \right)^{\beta} & 1 \leq \lambda_{n} \leq \lambda_{0} \\ E_{\text{lin}} \left(\lambda_{n} - \lambda_{0} \right) + B \left(\lambda_{n}^{2} - \lambda_{0}^{2} \right) + \frac{E_{\text{lin}}}{4\beta \left(\beta - 1 \right) \lambda_{0}^{3}} \left(\lambda_{0}^{2} - 1 \right)^{2} & \lambda_{n} > \lambda_{0} \end{cases} \tag{1} \end{split}$$

To account for potential AGE-modifiable fibrous AF crosslinking structures, non-enzymatic crosslinks were modeled as a combination of three possible components oriented in mutually perpendicular directions, including (1) in-plane crosslinks parallel to the collagen fibers (in-plane shear crosslinks), (2) in-plane crosslinks perpendicular to the collagen fibers (in-plane normal crosslinks), and (3) out-of-plane crosslinks oriented in the AF radial direction (outof-plane radial crosslinks; Fig. 1C). All crosslink components were modeled as extrafibrillar reinforcements described by the powerlinear fiber description (Eq. (1)). Since no previous evidence has pointed towards variations in crosslink mechanics with orientation, all crosslink components were assumed to share identical material parameters. Nonlinear crosslink material parameters (i.e., β and λ_0) were assigned the same values as the collagen fibers, with exception of the crosslink modulus ($E_{crosslink}$), which was the calibrated parameter in this study. A higher AGE content was assumed to generate a proportionally greater amount of AGEs that could crosslink collagen fibers, resulting in denser AGE compounds per specimen unit volume, and thus a higher apparent crosslink modulus (i.e., $E_{\text{crosslink, GLY50}} = 2 \times E_{\text{crosslink, GLY25}}$).

The adapted FEM was validated to ensure its predictive power over AF uniaxial tensile mechanics with non-enzymatic glycation. All validation FEMs were loaded in two steps. To account for specimen hydration, free-swelling was simulated in the SPEG5 external bath [27]. The post-swelling, pre-tension configuration was defined as the reference configuration for mechanics calculations. A uniaxial quasistatic tensile ramp to 40% engineering strain was then applied in the circumferential direction for the circumferential-axial and circumferential-radial models, while a uniaxial quasistatic tensile ramp to 150% radial engineering strain was simulated for the radial model. Displacement on the specimen top and bottom surfaces was constrained to the loading direction throughout the simulated tension. For the circumferential-axial and circumferentialradial models, the tensile modulus was calculated as the slope of the linear region of the engineering stress-strain curve between 25% and 35% engineering strain. The tensile modulus for the radial models was calculated as the slope of the engineering stress-strain response between 100% and 150% engineering strain. To ensure an optimal solution for the crosslink modulus calibration, a parametric study was conducted by developing parametric FEMs with varying crosslink modulus (n = 16 per orientation for circumferentialaxial and circumferential-radial models). Model predictions were considered valid if the predicted tensile modulus deviated from the respective reported experimental means by less than 50% of the reported standard deviation.

A multivariate linear regression model was used to evaluate the relationship between the increase in AF circumferential tensile modulus and crosslink modulus based on the parametric FEM models. Significance was assumed for p < 0.05. The relative contribution of crosslink modulus to the increase in AF circumferential tensile modulus was calculated using the relaimpo package in R and reported as a percentage [49].

2.2.2. Effect of non-enzymatic glycation on multiscale AF mechanics Following model validation, another set of circumferential-axial and circumferential-radial models was developed to investigate

the effect of non-enzymatic glycation on multiscale AF mechanics. While model dimensions still mimicked the samples for mechanical testing, the midlength notch geometry was excluded (Fig. 1D). Models were developed to represent the CTRL and GLY50 samples loaded under uniaxial and biaxial boundary conditions. For the uniaxial models, the boundary and loading conditions were identical to the validation FEMs. For the biaxial models, the axial boundaries were fixed throughout the simulated quasistatic tension, which was applied in the circumferential direction to 40% engineering strain (Fig. 1D). The post-swelling, pre-tension configuration was defined as the reference configuration. The apparent bulk tensile modulus was calculated as the slope of the linear region of the engineering stress-strain curve between 25% and 35% engineering strain. The average stress in the extrafibrillar matrix and fibers were evaluated throughout the simulated tension. The percentage of failed tissue elements was evaluated at 0.5 MPa circumferential stress due to physiologic relevance [40], which was calculated as the applied circumferential load divided by the respective specimen cross-sectional area. To ensure the robustness of our model predictions, the percentage of tissue failure was also evaluated using a strain-based assumption at 15% circumferential engineering strain, which corresponds to the largest internal AF strain observed in vitro in intact discs under physiologically relevant loadings [50,51]. Failure of individual tissue elements was assessed using a stress-based criterion. Bulk AF radial failure stress was considered representative of matrix failure stress due to the minimum fiber engagement in that orientation. The failure stress for the fibers was determined based on data in the literature [52]. The failure threshold was set at 75% of the respective mean failure stress to better represent tissue failure initiation following yielding [53].

3. Results

3.1. Experimental testing

Circumferential-radial specimens demonstrated a nonlinear bulk stress-strain response, while radial samples showed a pseudo-linear bulk stress-strain response prior to bulk tissue failure (Fig. 2 – colored solid lines). A clear linear region was observed for all circumferential-radial specimens (Fig. 2A – inset). A maximum stress that corresponded to bulk tissue failure was observed for all specimens. Mechanical testing data was only analyzed for samples that demonstrated a clean midlength failure (circumferential-radial: 73% of total specimens, n=11 per treatment group; radial: 88% of total specimens, n=7 per treatment group).

For circumferential-radial specimens, the GLY50 treatment increased the tensile modulus by 53% compared to the CTRL group (CTRL: 11.73 \pm 2.76 MPa, GLY50: 17.96 \pm 3.24 MPa, p < 0.001) and by 35% compared to the GLY25 group (GLY25: 13.33 \pm 4.95 MPa, p = 0.013; Fig. 3 - Circ-rad). The GLY50 treatment also increased the failure stress by 57% compared to the CTRL group (CTRL: 2.35 \pm 0.77 MPa, GLY50: 3.69 \pm 0.83 MPa, p < 0.001) and by 32% compared to the GLY25 group (GLY25: 2.79 ± 1.24 MPa, p = 0.012; Fig. 4A – Circ-rad). However, the tensile modulus and failure stress of the GLY25 samples were not different from the CTRL specimens (p > 0.35). For radial specimens, the GLY50 treatment increased the failure stress by 40% compared to the CTRL group (CTRL: 0.39 \pm 0.15 MPa, GLY50: 0.54 \pm 0.09 MPa, p = 0.043; Fig. 4A - Radial). However, the tensile modulus was not affected by the glycation treatment (p > 0.90; Fig. 3 – Radial). Non-enzymatic glycation did not affect tissue failure strain in both tested orientations and all treatment groups (p > 0.35; Fig. 4B). Additionally, a trend in failure energy ratio was not observed with non-enzymatic glyca-

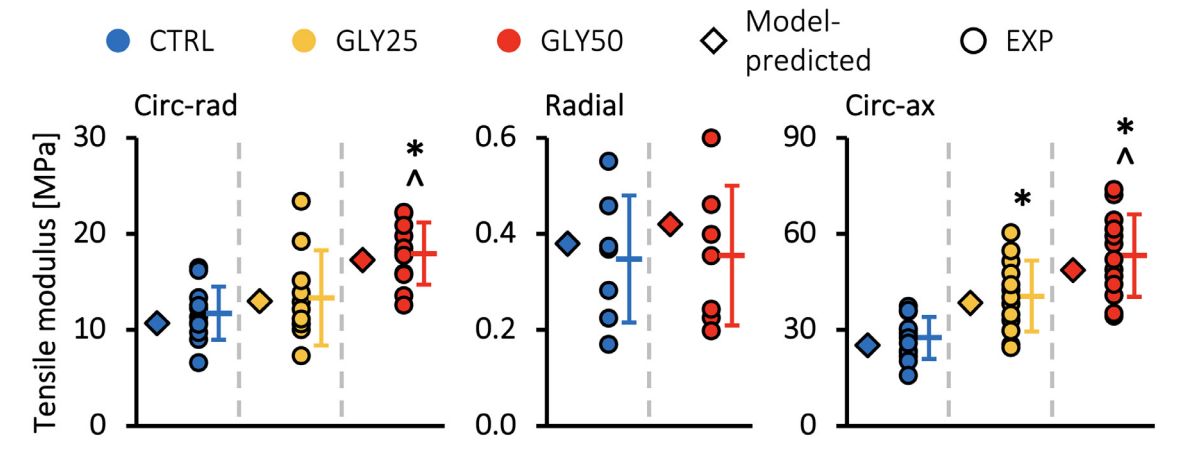


Fig. 3. Experimental tensile modulus (circles) compared to model predictions (diamonds) at each glycation level for all three specimen orientations. Data reported for circumferential-axial samples are reproduced from Werbner et al. for model validation [20]. * represents p < 0.001 vs. CTRL; ^ represents p < 0.05 vs. GLY25.

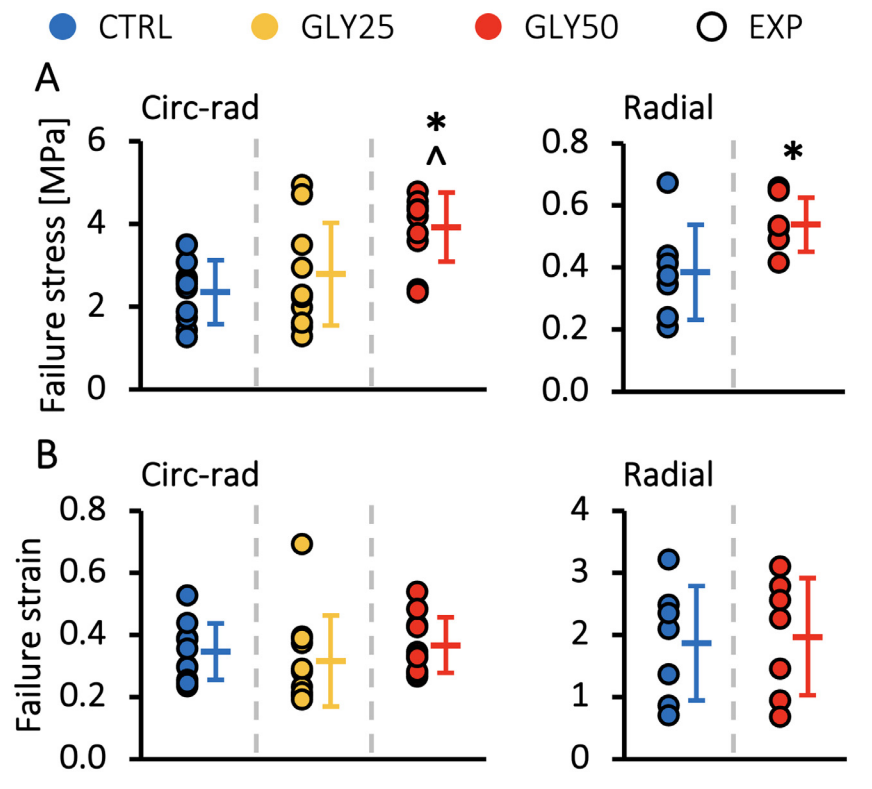


Fig. 4. (A) Failure stress and (B) failure strain at each glycation level for both specimen orientations. * represents p < 0.05 vs. CTRL; ^ represents p < 0.05 vs. GLY25.

AGE content normalized by tissue dry weight increased by 87% with the GLY25 treatment (CTRL: 250 ± 84 ngQ/mg dry weight; GLY25: 468 ± 138 ngQ/mg dry weight, p < 0.001) and by ~210% with the GLY50 treatment (GLY50: 779 ± 87 ngQ/mg dry weight, p < 0.001). The AGE content of the GLY50 group was ~65% higher than the GLY25 group (p < 0.001; Fig. 5A). Water and collagen content were not affected by the glycation treatment (Fig. 5B and 5C).

In the circumferential-radial direction, there was a moderate positive correlation between AGE content and tensile modulus (R = 0.55, p < 0.001; Fig. 6A – black trendline); a moderate positive correlation was also observed between AGE content and failure stress (R = 0.55, p < 0.0001; Fig. 6B – black trendline). Specimen orientation had a significant effect on the relationship between AGE content and tensile modulus and between AGE content and failure stress (ANCOVA p < 0.001), with the tensile properties

of circumferential-axial specimens being more sensitive to AGE accumulation (Fig. 6 – gray vs. black trendlines).

3.2. Finite element modeling

3.2.1. Model validation

With all three possible crosslink components (i.e., in-plane shear crosslinks, in-plane normal crosslinks, and out-of-plane radial crosslinks, Fig. 1C), model predictions showed that a crosslink modulus lower than 0.1 MPa was required to predict an AF radial tensile modulus within the range of existing experimental data (Fig. 7A). Meanwhile, FEMs with a crosslink modulus of 10 MPa predicted an AF radial tensile modulus of 6.38 MPa, more than $10\times$ higher than the largest AF radial tensile modulus reported (Fig. 7A). However, a crosslink modulus greater than 7.5

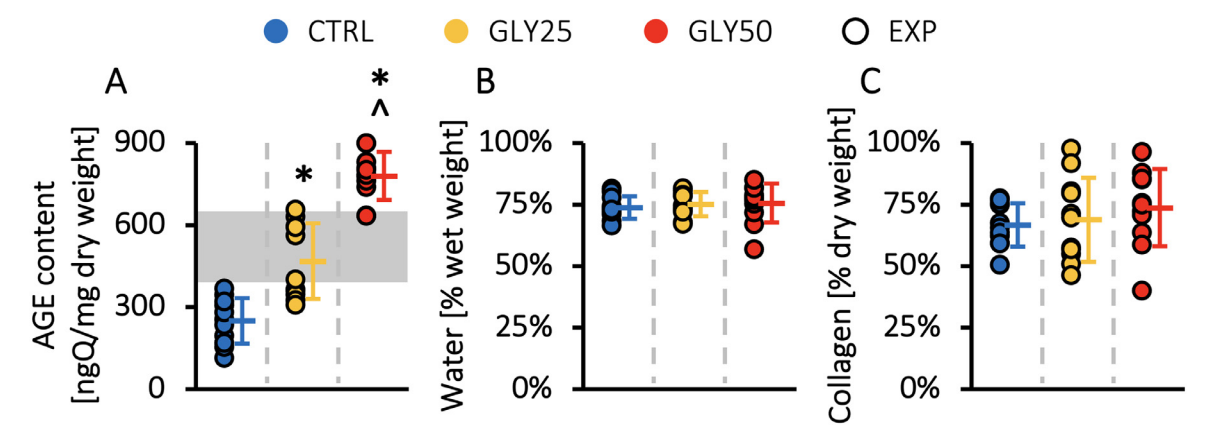


Fig. 5. (A) AGE, (B) water, and (C) collagen content at each glycation level. The gray region in (A) represents the range of AGE content measured in human discs [20]. * represents p < 0.001 vs. CTRL; ^ represents p < 0.001

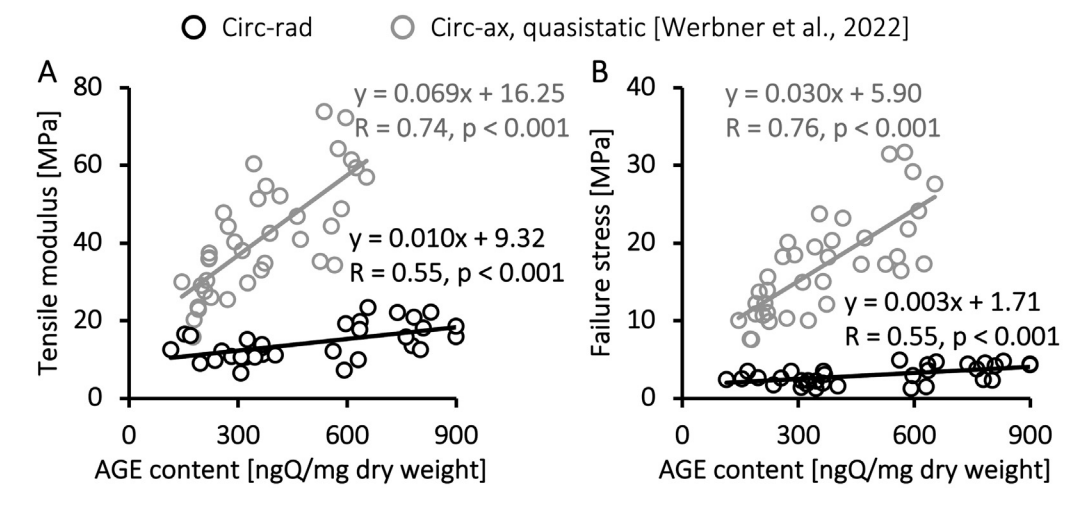


Fig. 6. Bivariate linear correlation between **(A)** tensile modulus and **(B)** failure stress and AGE content for circumferential-radial samples (black circles). Quasistatic circumferential-axial data reported by Werbner et al. were shown for comparison (gray circles) [20]. Regression models obtained for the two specimen orientations were significantly different (ANCOVA p < 0.001).

MPa was required to generate model predictions within approximately one standard deviation of the mean circumferential tensile modulus values (Fig. 7B). Therefore, out-of-plane radial crosslinks were not included in the model (Fig. 1C). Model predictions also showed that FEMs with only in-plane shear crosslinks or in-plane normal crosslinks greatly underestimated AF circumferential tensile modulus for the GLY50 group (Fig. 7C). Thus, both in-plane shear crosslinks and in-plane normal crosslinks were necessary and therefore included in the model.

Adapted FEMs accurately and robustly predicted experimental measurements when the crosslink modulus was 12.5% of collagen fibers (i.e., 7.5 MPa) in the GLY25 model and 25% of collagen fibers (i.e., 15 MPa) in the GLY50 model, which was further confirmed by the parametric FEM predictions (Fig. 7B). Model predictions matched well with experimental stress-strain responses in all specimen orientations and all treatment groups (Fig. 2 – colored dashed vs. solid lines). Model-predicted bulk AF tensile modulus values were within 0.4 \times standard deviation from the experimental means in all specimen orientations and all treatment groups (Fig. 3). Thus, the adapted FEMs were considered valid for describing and investigating AF tensile mechanics with non-enzymatic glycation.

Multivariate linear regression models were able to explain more than 99.5% of the variance in parametric FEMs. Terms associated with the out-of-plane radial crosslinks were excluded from the models. The increase in AF circumferential tensile modulus increased linearly with in-plane shear and in-plane normal crosslink modulus (p < 0.001 for both crosslink types and specimen orientations) but did not depend on their interactions (Eqs. (2) and (3)). The relative contribution analysis suggested that the increase in AF circumferential tensile modulus was more sensitive to the in-plane shear than the in-plane normal crosslink modulus. Particularly, the in-plane shear crosslink modulus contributed to $\sim\!90\%$ of the increase in circumferential tensile modulus in both orientations, while the in-plane normal crosslink modulus only contributed $\sim\!10\%$.

$$\Delta E_{\text{Circ-ax}} = 4.62 + 0.91 \times E_{\text{crosslink, ISC}} + 0.27 \times E_{\text{crosslink, INC}} + \varepsilon$$
(2)

$$\Delta E_{\text{Circ-rad}} = 0.21 + 0.41 \times E_{\text{crosslink, ISC}} + 0.13 \times E_{\text{crosslink, INC}} + \varepsilon$$
(3)

3.2.2. Effect of non-enzymatic glycation on multiscale AF mechanics
For circumferential-axial models, the biaxial boundary condition increased the apparent tensile modulus by 62-85% (Fig. 8A – Circ-ax, diagonal vs. solid bars). Glycation had a comparable effect,

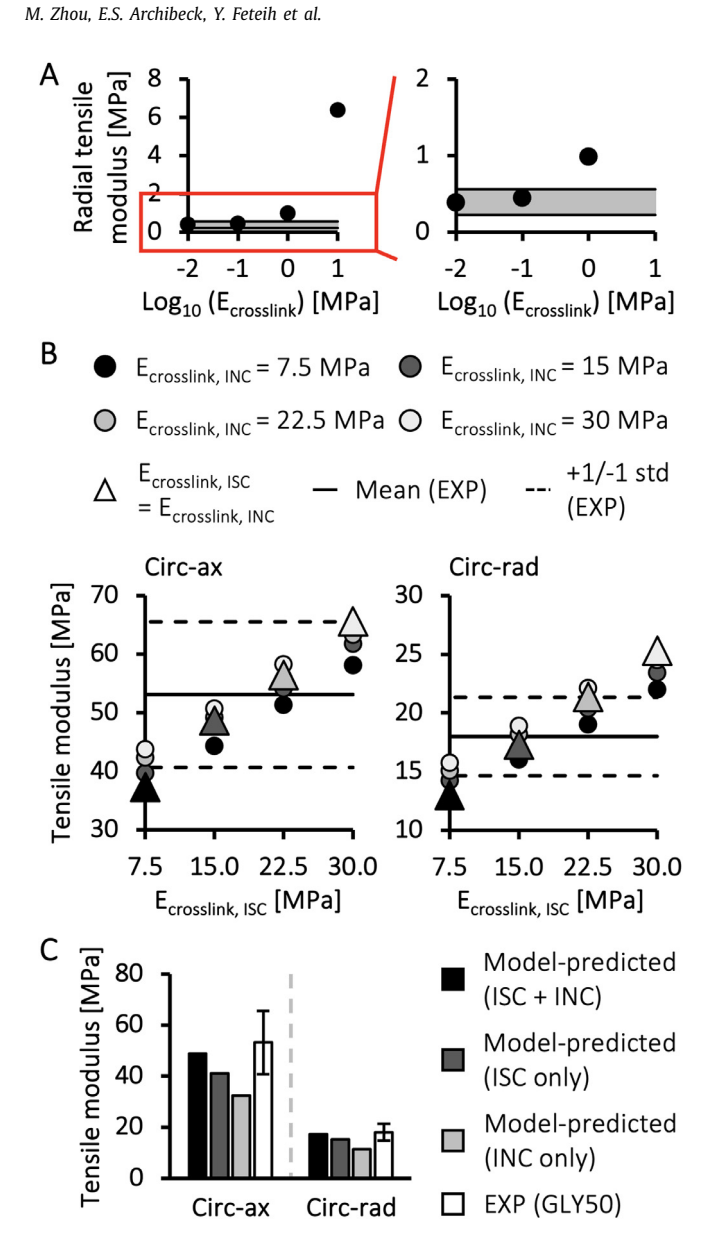


Fig. 7. (A) Model-predicted AF radial tensile modulus with varying crosslink modulus ($E_{\rm crosslink}=0.01$ MPa, 0.1 MPa, 1 MPa, and 10 MPa). Predicted values were compared to the AF radial tensile modulus range reported in the literature, highlighted by the gray region [40,54–56]. **(B)** Model-predicted tensile modulus for circumferential-axial and circumferential-radial specimens with varying crosslink modulus. Horizontal solid and dashed lines represent the range of experimental data (mean \pm standard deviation, std). **(C)** Model-predicted circumferential tensile modulus for GLY50 specimens with varying crosslinking structures vs. experimental data.

increasing the apparent tensile modulus by 66-89% (Fig. 8A – Circax, red vs. blue bars). For circumferential-radial models, the biaxial boundary condition had a less pronounced effect, only increasing the apparent tensile modulus by 17-28% (Fig. 8A – Circ-rad, diagonal vs. solid bars); however, glycation increased the apparent tensile modulus by more than 75% (Fig. 8A – Circ-rad, red vs. blue bars).

Model predictions indicated that glycation had a greater impact on subtissue-level mechanics than altered boundary conditions, especially in the extrafibrillar matrix (Figs. 8B, 8C, and 9). Under 0.5 MPa, the average matrix stress in the uniaxial circumferential-axial CTRL model was 0.25 MPa and increased by \sim 60% to 0.40 MPa with glycation (Fig. 8B – Matrix, solid blue vs. red lines; Fig. 9A). Simulating a biaxial boundary condition only increased the average

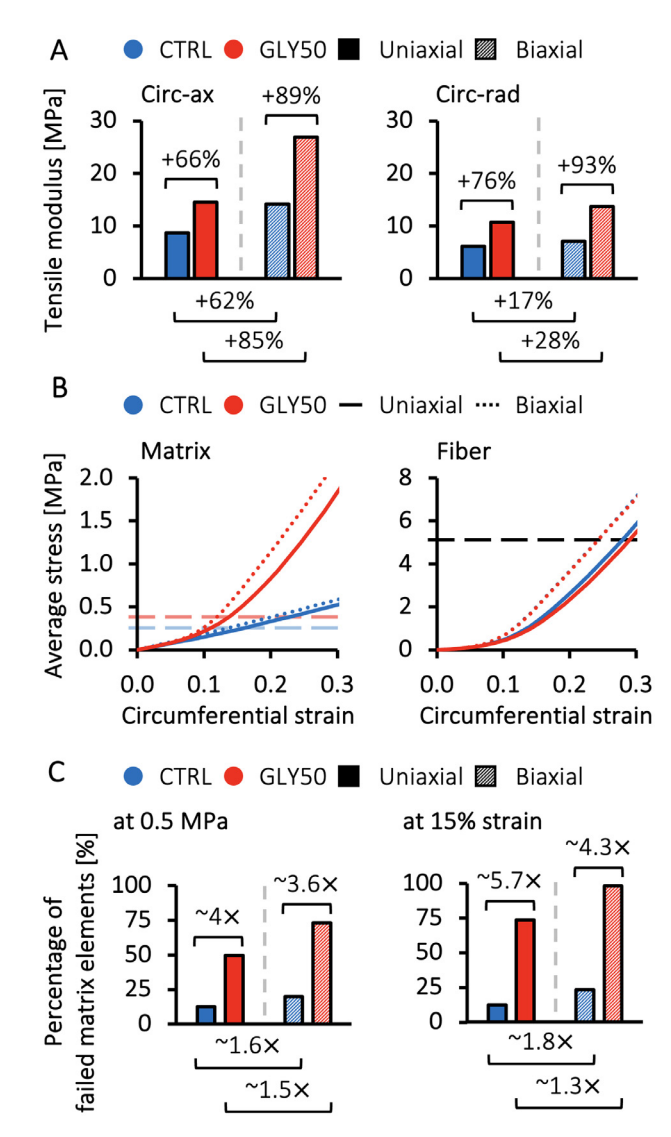


Fig. 8. Model-predicted **(A)** circumferential tensile apparent modulus, **(B)** average matrix and fiber stress. The light blue and red horizontal dashed lines represent the stress thresholds for failed matrix elements in CTRL and GLY50 models, respectively. The black dashed line represents the failure stress threshold for fibers [52]. **(C)** Percentage of failed matrix elements evaluated at 0.5 MPa circumferential stress and 15% engineering strain. (For interpretation of the references to colour in this figure legend, the reader is referred to the web version of this article.)

matrix stress by less than 5% (Fig. 8B – Matrix, blue solid vs. dotted lines; Fig. 9A). Based on the failure criterion calculated using the measured AF radial failure stress (CTRL: 0.39 MPa \times 75% = 0.29 MPa; GLY50: 0.54 MPa \times 75% = 0.40 MPa; Fig. 4A), glycation led to a \sim 4 \times increase in the percentage of failed matrix elements from 13% to 50% under uniaxial tension at 0.5 MPa (Fig. 8C – red vs. blue solid bars), while biaxial loading resulted in a \sim 1.5 \times increase in the percentage of failed matrix elements (Fig. 8C – diagonal vs. solid blue bars). In the circumferential-axial biaxial models, glycation increased the average matrix stress by \sim 90% from 0.30 to 0.56 MPa (Fig. 8B – Matrix, dotted blue vs. red lines; Fig. 9A), resulting in over 70% of the matrix elements exceeding the failure threshold (Fig. 8C – at 0.5 MPa, diagonal red bar). A similar trend was observed when evaluating failure using a strain-controlled assumption at 15% engineering strain (Fig. 8C – at 15% strain; Fig. 9B).

Contrary to the changes in matrix mechanics, the average fiber stress was largely unaffected by glycation (Fig. 8B – Fiber, red vs. blue lines; Fig. 9). At 0.5 MPa circumferential stress or 15% engi-

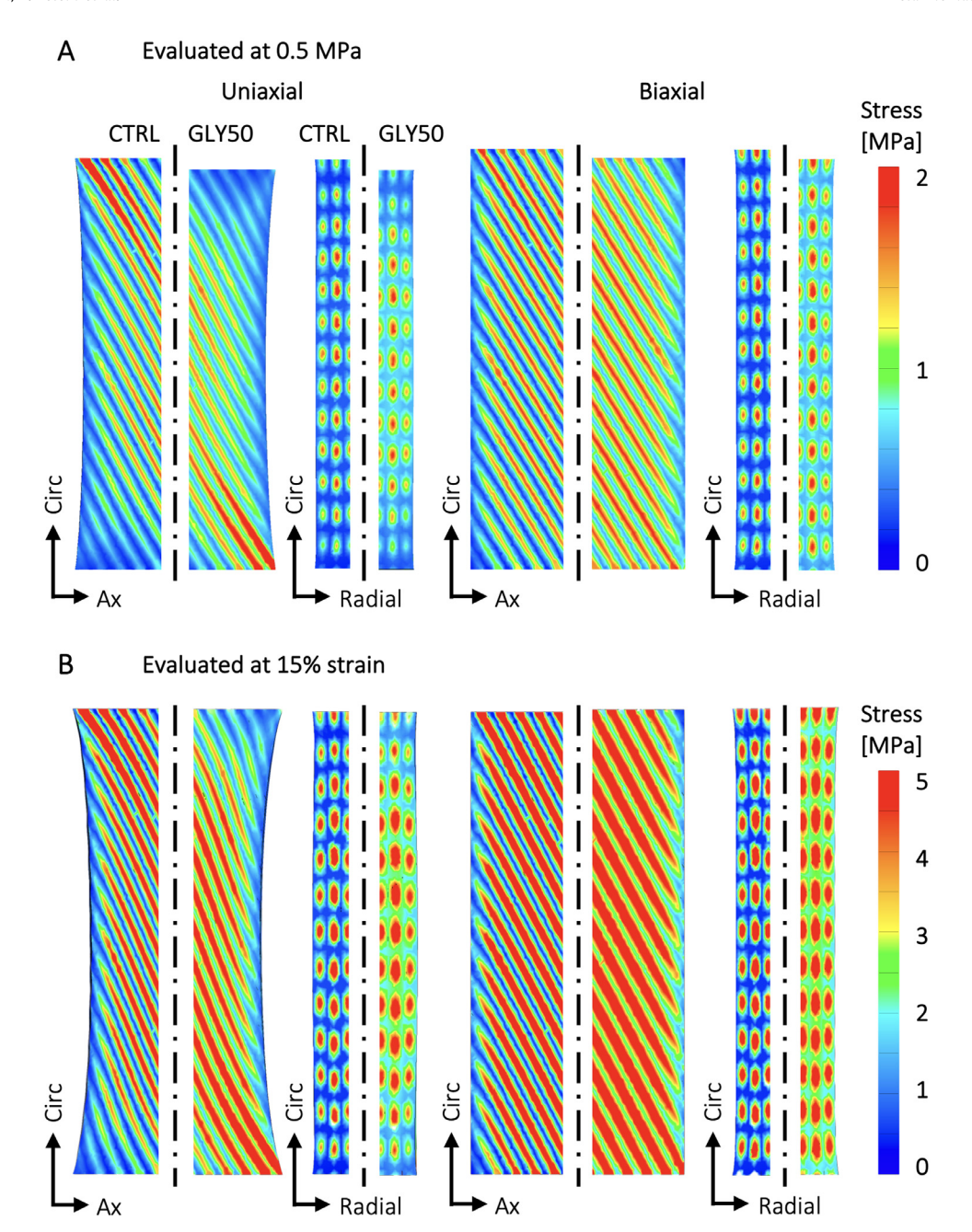


Fig. 9. (A) Representative frontal and side midplane stress distributions at 0.5 MPa circumferential stress for CTRL and GLY50 models. Stress in the extrafibrillar matrix increased with glycation, changing from dark blue shading in the CTRL to green in the GLY50 models. Red shadings represent higher stresses in the fibers (vs. the matrix). **(B)** Representative stress distributions at 15% applied circumferential engineering strain showed a similar trend.

neering strain, increasing the boundary constraints with the biaxial boundary increased the average fiber stress by 20-70%, but the average fiber stress remained well below the failure threshold (Fig. 8B – Fiber, solid vs. dotted lines). A similar trend was observed for models oriented in the circumferential-radial direction.

4. Discussion

The study investigated the relationship between physiologic levels of advanced glycation end-products and anisotropic AF uniaxial tensile mechanics using a combined experimental-computational approach. *In vitro* glycation increased AF tensile modulus and failure stress in the circumferential-radial direction (Figs. 3 and 4A), agreeing with previous observations reported for circumferential-axial samples [19,20]. However, for circumferential-

radial specimens, changes in tensile mechanics with AGE accumulation were not as pronounced (Fig. 6) [20]. Specifically, the *in vitro* glycation treatments led to comparable increases in AGE content in both specimen orientations [20]. However, the GLY50 treatment increased the AF tensile modulus and failure stress by $\sim\!100\%$ for the circumferential-axial specimens but only by $\sim\!50\%$ for the circumferential-radial specimens. While the GLY25 treatment led to statistically significant increases in circumferential-axial tensile modulus and failure stress, it did not affect the circumferential-radial specimens (Figs. 3 and 4A). Additionally, multivariate linear regression predicted that the modulus of in-plane shear crosslinks, which are parallel to the collagen fibers, contributed to approximately 90% of the increase in tensile modulus. The primary distinction between circumferential-axial and circumferential-radial specimens lies in the loading direction relative to the orientation and

length of the collagen fibers. In particular, collagen fibers in the circumferential-radial specimen extended across the 2 mm thickness, while fibers in the circumferential-axial sample traversed the entire 5 mm width, resulting in a larger effective fiber length and fiber engagement [29,57]. Taken together, these findings indicated that non-enzymatic crosslinks had the greatest impact along the collagen fiber direction, with this effect increasing with intact fiber length and fiber engagement.

Non-enzymatic glycation had a smaller effect on AF radial mechanics, where fiber engagement was minimal during loading. Specifically, the GLY50 treatment did not affect the tissue modulus and only increased the failure stress by 40% (Figs. 3 and 4A). FEM predictions also suggested a negligible effect from the AGEs in the radial direction (Fig. 1C), as including out-of-plane radial crosslinks led to unrealistically high radial tensile modulus (Fig. 7A). While defining a smaller modulus for the radial crosslinks (i.e., 0.01-0.1 MPa) compared to the in-plane crosslinks produced realistic AF radial tensile modulus predictions (Fig. 7A), we did not find previous evidence supporting stiffness variations between AGEs compounds derived from the same collagen type. Previous two-dimensional constitutive models developed to describe AF mechanics with glycation also suggested that in-plane crosslinks were sufficient [18]. Furthermore, elastin proteins, the main constituents of interlamellar elastic fibers oriented in the AF radial direction, only accounted for 2% of tissue dry weight, indicating a low likelihood of elastinderived AGEs compounds (i.e., out-of-plane radial crosslinks) [58-60]. A multiphoton autofluorescence study further complemented these findings by demonstrating that collagens were more responsive to AGE formation than interlamellar elastic fibers [61]. Thus, our results agree with and add to the existing literature regarding the crosslinking structure by showing that interlamellar radial crosslinks are unlikely to form in the AF.

Studies that evaluate mechanical properties of human disc soft tissues are known to report large variations. While reported mechanics variations between studies can be attributed to differences in specimen geometry [29], variations within studies might, in part, be due to differences in tissue composition with degeneration and disease. For example, coefficients of variation (i.e., the ratio of the standard deviation to the mean) for the tensile modulus of healthy anterior outer circumferential-axial AF specimens, whose structure and morphology are expected to be relatively uniform, still range from 0.56 to 0.82 [53,55,56,62]. This study evaluated a parametric group of crosslink modulus values corresponding to different AGE levels to determine the effect of AGE accumulation on bulk tissue mechanics. The parametric models predicted a range of modulus values that spanned the experimental variations reported in both specimen orientations (Fig. 7B). This finding suggested that large variations observed in human disc mechanical properties may be in part due to variations in AGE content, which are often not accounted for during tissue degeneration level evaluations (e.g., Thompson scale) [63].

AGE accumulation occurs naturally with aging and has been linked to various soft tissue diseases besides disc degenerative disorders, such as osteoarthritis and tendinopathy [15,64,65]. Studies using diabetic rodent models also reported significantly reduced tendon modulus and failure stress [66,67]. However, conflicting results have been reported *in vitro*. In addition to the increased AF energetic toughness reported in the current and previous AF studies [18–20], non-enzymatic glycation *in vitro* has been found to increase tissue stiffness and failure stress in other soft fiber-reinforced soft tissues, such as tendons, cartilages, and corneas [68–72]. *In vitro* crosslinking also enhanced tissue resistance to collagen degradation and mechanical wear [73]. Researchers have partially attributed this discrepancy to the uncoupling of exogenous AGE accumulation from natural cellular and tissue remodeling in response to a high AGE extracellular environment, which is known

to induce cellular inflammatory responses [24,74–77]. Alternatively, tendon studies reported that AGE treatment significantly reduced tissue viscoelastic properties (i.e., energy dissipation capabilities) [69,70], suggesting that diabetic crosslinking might induce premature tissue failure by compromising tissue performance under fatigue loading. Additionally, tendon studies have shown that nonenzymatic glycation may result in tissue stiffening due to diminished interfibrillar sliding [69,70,72,78]. Similar mechanisms may be at play in the AF, despite the differences in tissue composition and fiber orientation; however, interfibrillar sliding was beyond the scope of this study.

In this study, subtissue-level FEM predictions provided another probable explanation for this discrepancy between in vivo and in vitro tissue failure behavior with AGE accumulation. Under a physiologically relevant stress (i.e., \sim 0.5 MPa) or strain range (i.e., \leq 15% strain), glycation greatly increased the stress in the extrafibrillar matrix, predisposing a larger portion of the tissue to a greater risk of mechanical failure (Fig. 8B and C). The current study evaluated matrix failure under both stress- and strain-controlled methods, as both approaches have been used frequently and interchangeably in experimental and computational studies [79]. As such, the improved bulk AF tensile mechanical properties with AGE accumulation were achieved at the risk of exposing the extrafibrillar matrix to increased mechanical damage accumulation. Additionally, previous cellular biology studies showed that higher stresses applied to AF cells caused inflammatory responses, which may also trigger premature tissue failure through catabolic remodeling [80–82]. Lastly, future experimental work is needed to confirm that findings from this study are translatable to human disc tissues.

The biaxial boundary condition was simulated in the current study due to its physiologic relevance and difficulties in conducting repeatable soft tissue biaxial tensile testing *in vitro*. Model predictions highlighted that glycation had a greater effect on AF bulk and subtissue-level mechanics than the evaluated biaxial boundary condition (i.e., an axial-fixed condition), especially on the stresses in the extrafibrillar matrix (Fig. 8B). However, the more constrained biaxial boundary amplified the effect of glycation, disposing nearly all the matrix elements in the GLY50 biaxial model to failure under large physiologic deformations (Fig. 8C). This amplifying effect may be more pronounced *in vivo*, as the heavily glycated tissues would be more restricted by the surrounding structures (e.g., the nucleus and endplates), further increasing the risk of tissue failure.

One limitation of the current study was that tissue proteoglycan content was not characterized. However, previous in vitro studies consistently reported that AGE treatment did not affect proteoglycan content, regardless of the crosslinking agent used [83-85]. Tissue water content, a benchmark for proteoglycan content, also remained at the fresh tissue level for all treatment groups (Fig. 5B), suggesting that proteoglycan was unaffected by the methylglyoxalbased treatment. While AGE content in discs from diabetic patients has not been characterized, the AGE content induced in GLY25 specimens aligned well with the range measured from human cadaveric disc tissues, while CTRL and GLY50 specimens covered the lower and higher end of that range (Fig. 5A) [20], making our specimens justifiable candidate tissue models to examine the differences between healthy and diabetic tissues. Another limitation was that the current study did not characterize the elastin-derived AGE content, which could have a considerable effect on AF mechanics, especially with degeneration [59]. Computationally, crosslinks were described as extrafibrillar reinforcements. Future models may need to explicitly describe crosslinks to differentiate failure originating from the extrafibrillar matrix from the crosslinks themselves. This differentiation could highlight the relative contribution of fiber stiffening and reduced interfibrillar sliding to bulk tissue strengthening with glycation, which remains a debate in the field [69,70,72,78].

JID: ACTBIO [m5G;July 13, 2023;16:12]

M. Zhou, E.S. Archibeck, Y. Feteih et al.

5. Conclusions

The current study evaluated the effects of AGEs on anisotropic AF uniaxial tensile mechanics using a combined experimentalcomputational approach. Experimentally, AF uniaxial tensile mechanical properties were reported in circumferential-radial and radial directions at three physiologically relevant AGE levels. Computationally, multiscale structure-based FEMs were developed and validated to describe crosslinks within the extrafibrillar matrix. The validated models were used to examine the effect of glycation on multiscale AF mechanics under uniaxial and biaxial boundary conditions. Mechanical testing results showed that in vitro glycation did not lead to compromised AF mechanical properties under monotonic quasistatic uniaxial tension in both tested orientations, agreeing with previous literature. The proposed FEM framework accurately predicted AF bulk tensile mechanics with glycation and provided insight into the relationship between AGE accumulation and more frequent and severe tissue failure observed with diabetes. Specifically, glycation exposed the extrafibrillar matrix to greater stresses under physiologically relevant deformations, which may lead to increased tissue failure through greater accumulated mechanical damage or catabolic tissue remodeling. Our findings also suggested probable crosslinking structures at the subtissue level, indicating that AGEs had a more pronounced effect along the fiber direction, while interlamellar radial crosslinks were less likely to form in the AF. In conclusion, the improved bulk mechanical properties of fiber-reinforced biological tissues with AGE accumulation may be achieved at the risk of exposing the extrafibrillar matrix to larger stresses under physiologic deformations, leading to premature tissue failure. The presented combined approach provides a powerful tool for examining multiscale AF structurefunction relationships with disease progression, which is crucial for developing effective preventive measures and therapeutic interventions for low back pain.

Declaration of Competing Interest

The authors declare that they have no known competing financial interests or personal relationships that could have appeared to influence the work reported in this paper.

Acknowledgements

This work was supported by National Science Foundation [CA-REER #1751212 - GDO; GRFP #DGE 2146752 - ESA].

This material is based upon work supported by the National Science Foundation Graduate Research Fellowship Program under Grant No. DGE 2146752. Any opinions, findings, and conclusions or recommendations expressed in this material are those of the author(s) and do not necessarily reflect the views of the National Science Foundation.

The authors would like to express their graditude to Dr. Benjamin Werbner for his valuable guidance and training in mechanical testing and biochemical assays.

Supplementary materials

Supplementary material associated with this article can be found, in the online version, at doi:10.1016/j.actbio.2023.07.003.

References

- [1] D. Hoy, L. March, P. Brooks, F. Blyth, A. Woolf, C. Bain, G. Williams, E. Smith, T. Vos, J. Barendregt, C. Murray, The global burden of low back pain: estimates from the Global Burden of Disease 2010 study, Ann. Rheum. Dis. 73 (6) (2014) 968–974.
- [2] D.E. Bloom, A. Boersch-Supan, P. McGee, A. Seike, Population aging: facts, challenges, and responses, Benefits Compens. Int. 41 (1) (2011) 22.

[3] B.M. Popkin, Nutrition transition and the global diabetes epidemic, Curr. Diabetes Rep. 15 (2015) 1–8.

Acta Biomaterialia xxx (xxxx) xxx

- [4] B. Zhou, Y. Lu, K. Hajifathalian, J. Bentham, M. Di Cesare, G. Danaei, H. Bixby, M.J. Cowan, M.K. Ali, C. Taddei, W.C. Lo, Worldwide trends in diabetes since 1980: a pooled analysis of 751 population-based studies with 4-4 million participants. Lancet N. Am. Ed. 387 (10027) (2016) 1513–1530.
- ticipants, Lancet N. Am. Ed. 387 (10027) (2016) 1513–1530.
 [5] A.M. Jakoi, G. Pannu, A. D'oro, Z. Buser, M.H. Pham, N.N. Patel, P.C. Hsieh, J.C. Liu, F.L. Acosta, R. Hah, J.C. Wang, The clinical correlations between diabetes, cigarette smoking and obesity on intervertebral degenerative disc disease of the lumbar spine, Asian Spine J. 11 (3) (2017) 337.
- [6] X. Liu, F. Pan, Z. Ba, S. Wang, D. Wu, The potential effect of type 2 diabetes mellitus on lumbar disc degeneration: a retrospective single-center study, J. Orthop. Surg. Res. 13 (1) (2018) 1–5.
- [7] T. Steelman, L. Lewandowski, M. Helgeson, K. Wilson, C. Olsen, D. Gwinn, Population-based risk factors for the development of degenerative disk disease, Clin. Spine Surg. 31 (8) (2018) E409–E412.
- [8] F. Russo, L. Ambrosio, K. Ngo, G. Vadalà, V. Denaro, Y. Fan, G. Sowa, J.D. Kang, N. Vo, The role of type I diabetes in intervertebral disc degeneration, Spine 44 (17) (2019) 1177.
- [9] B.S. Jhawar, C.S. Fuchs, G.A. Colditz, M.J. Stampfer, Cardiovascular risk factors for physician-diagnosed lumbar disc herniation, Spine J. 6 (6) (2006) 684–691.
- [10] P.P. Raj, Intervertebral disc: anatomy-physiology-pathophysiology-treatment, Pain Pract. 8 (1) (2008) 18–44.
- [11] M.A. Adams, P.J. Roughley, What is intervertebral disc degeneration, and what causes it? Spine 31 (18) (2006) 2151–2161.
- [12] P.P. Vergroesen, I. Kingma, K.S. Emanuel, R.J. Hoogendoorn, T.J. Welting, B.J. van Royen, J.H. van Dieën, T.H. Smit, Mechanics and biology in intervertebral disc degeneration: a vicious circle, Osteoarthr. Cartil. 23 (7) (2015) 1057–1070.
- [13] H. Vlassara, M.R. Palace, Diabetes and advanced glycation endproducts, J. Intern. Med. 251 (2) (2002) 87–101.
- [14] N. Ahmed, P.J. Thornalley, Advanced glycation endproducts: what is their relevance to diabetic complications? Diabetes Obes. Metab. 9 (3) (2007) 233–245.
- [15] A. Suzuki, A. Yabu, H. Nakamura, Advanced glycation end products in musculoskeletal system and disorders, Methods, 203 (2022) 179–186.
- [16] N. Verzijl, J. DeGroot, S.R. Thorpe, R.A. Bank, J.N. Shaw, T.J. Lyons, J.W. Bijlsma, F.P. Lafeber, J.W. Baynes, J.M. TeKoppele, Effect of collagen turnover on the accumulation of advanced glycation end products, J. Biol. Chem. 275 (50) (2000) 39027–39031.
- [17] J.G. Snedeker, A. Gautieri, The role of collagen crosslinks in ageing and diabetes-the good, the bad, and the ugly, Muscles Ligaments Tendons J. 4 (3) (2014) 303.
- [18] D.R. Wagner, K.M. Reiser, J.C. Lotz, Glycation increases human annulus fibrosus stiffness in both experimental measurements and theoretical predictions, J. Biomech. 39 (6) (2006) 1021–1029.
- [19] S.Y. Chuang, R.M. Odono, T.P. Hedman, Effects of exogenous crosslinking on *in vitro* tensile and compressive moduli of lumbar intervertebral discs, Clin. Biomech. 22 (1) (2007) 14–20.
- [20] B. Werbner, M. Lee, A. Lee, L. Yang, M. Habib, A.J. Fields, G.D. O'Connell, Non-enzymatic glycation of annulus fibrosus alters tissue-level failure mechanics in tension, J. Mech. Behav. Biomed. Mater. 126 (2022) 104992.
- [21] T.P. Hedman, H. Saito, C. Vo, S.Y. Chuang, Exogenous cross-linking increases the stability of spinal motion segments, Spine 31 (15) (2006) E480–E485.
- [22] A. Barbir, A.J. Michalek, R.D. Abbott, J.C. Iatridis, Effects of enzymatic digestion on compressive properties of rat intervertebral discs, J. Biomech. 43 (6) (2010) 1067–1073.
- [23] B.C. Kirking, J.K. Toungate, T.P. Hedman, The dose response relationship between intervertebral disc flexion-extension neutral zone metrics and injected genipin concentration, J. Appl. Biomater. Funct. Mater. 11 (2) (2013) 73–79.
- [24] A.J. Fields, B. Berg-Johansen, L.N. Metz, S. Miller, B. La, E.C. Liebenberg, D.G. Coughlin, J.L. Graham, K.L. Stanhope, P.J. Havel, J.C. Lotz, Alterations in intervertebral disc composition, matrix homeostasis and biomechanical behavior in the UCD-T2DM rat model of type 2 diabetes, J. Orthop. Res. 33 (5) (2015) 738–746.
- [25] D. Krishnamoorthy, R.C. Hoy, D.M. Natelson, O.M. Torre, D.M. Laudier, J.C. latridis, S. Illien-Jünger, Dietary advanced glycation end-product consumption leads to mechanical stiffening of murine intervertebral discs, Dis. Models Mech. 11 (12) (2018) p.dmm036012.
- [26] B. Werbner, M. Zhou, G. O'Connell, A novel method for repeatable failure testing of annulus fibrosus, J. Biomech. Eng. 139 (11) (2017) 111001.
- [27] B. Werbner, M. Zhou, N. McMindes, A. Lee, M. Lee, G.D. O'Connell, Saline-polyethylene glycol blends preserve in vitro annulus fibrosus hydration and mechanics: an experimental and finite-element analysis, J. Mech. Behav. Biomed. Mater. 125 (2022) 104951.
- [28] M. Zhou, S.E. Bezci, G.D. O'Connell, Multiscale composite model of fiber-reinforced tissues with direct representation of sub-tissue properties, Biomech. Model. Mechanobiol. 19 (2020) 745–759.
- [29] M. Zhou, B. Werbner, G.D. O'Connell, Fiber engagement accounts for geometry-dependent annulus fibrosus mechanics: a multiscale, Structure-Based Finite Element Study, J. Mech. Behav. Biomed. Mater. 115 (2021) 104292.
- [30] M. Zhou, S. Lim, G.D. O'Connell, A robust multiscale and multiphasic structure-based modeling framework for the intervertebral disc, Front. Bioeng. Biotechnol. 9 (2021) 685799.
- [31] M. Zhou, R.D. Huff, Y. Abubakr, G.D. O'Connell, Torque-and muscle-driven flexion induce disparate risks of *in vitro* herniation: a multiscale and multiphasic structure-based finite element study, J. Biomech. Eng. 144 (6) (2022) 061005.

ARTICLE IN PRESS

JID: ACTBIO [m5G;July 13, 2023;16:12]

M. Zhou, E.S. Archibeck, Y. Feteih et al.

- [32] C.N. Demers, J. Antoniou, F. Mwale, Value and limitations of using the bovine tail as a model for the human lumbar spine. Spine 29 (24) (2004) 2793–2799.
- [33] G.D. O'Connell, E.J. Vresilovic, D.M. Elliott, Comparison of animals used in disc research to human lumbar disc geometry, Spine 32 (3) (2007) 328–333.
 [34] S.E. Bezci, B. Werbner, M. Zhou, K.G. Malollari, G. Dorlhiac, C. Carraro,
- [34] S.E. Bezzi, B. Werbner, M. Zhou, K.G. Malollari, G. Doriniac, C. Carraro, A. Streets, G.D. O'Connell, Radial variation in biochemical composition of the bovine caudal intervertebral disc, JOR Spine 2 (3) (2019) e1065.
- [35] J. Yu, U. Tirlapur, J. Fairbank, P. Handford, S. Roberts, C.P. Winlove, Z. Cui, J. Urban, Microfibrils, elastin fibres and collagen fibres in the human intervertebral disc and bovine tail disc, J. Anat. 210 (4) (2007) 460–471.
- [36] D. Taylor, N. O'Mara, E. Ryan, M. Takaza, C. Simms, The fracture toughness of soft tissues, J. Mech. Behav. Biomed. Mater. 6 (2012) 139–147.
- [37] A.P. Hollander, T.F. Heathfield, C. Webber, Y. Iwata, R. Bourne, C. Rorabeck, A.R. Poole, Increased damage to type II collagen in osteoarthritic articular cartilage detected by a new immunoassay, J. Clin. Investig. 93 (4) (1994) 1722–1732.
- [38] F. Marchand, A.M. Ahmed, Investigation of the laminate structure of lumbar disc anulus fibrosus, Spine 15 (5) (1990) 402–410.
 [39] M.L. Schollum, P.A. Robertson, N.D. Broom, How age influences unravelling
- [39] M.L. Schollum, P.A. Robertson, N.D. Broom, How age influences unravelling morphology of annular lamellae-a study of interfibre cohesivity in the lumbar disc, J. Anat. 216 (3) (2010) 310-319.
- [40] G.A. Holzapfel, C.A. Schulze-Bauer, G. Feigl, P. Regitnig, Single lamellar mechanics of the human lumbar anulus fibrosus, Biomech. Model. Mechanobiol. 3 (2005) 125–140.
- [41] S.J. Matcher, C.P. Winlove, S.V. Gangnus, The collagen structure of bovine intervertebral disc studied using polarization-sensitive optical coherence tomography, Phys. Med. Biol. 49 (7) (2004) 1295.
- [42] S.A. Maas, B.J.Ellis, G.A. Ateshian J.A. Weiss, 2012. FEBio: finite elements for biomechanics.
- [43] W.M. Lai, J.S. Hou, V.C. Mow, 1991. A triphasic theory for the swelling and deformation behaviors of articular cartilage.
- [44] J.P.G. Urban, A. Maroudas, The measurement of fixed charged density in the intervertebral disc, Biochim. Biophys. Acta (BBA) Gen. Subj. 586 (1) (1979) 166–178.
- [45] J. Antoniou, T. Steffen, F. Nelson, N. Winterbottom, A.P. Hollander, R.A. Poole, M. Aebi, M. Alini, The human lumbar intervertebral disc: evidence for changes in the biosynthesis and denaturation of the extracellular matrix with growth, maturation, ageing, and degeneration, J. Clin. Investig. 98 (4) (1996) 996–1003.
- [46] L. Cao, F. Guilak, L.A. Setton, Pericellular matrix mechanics in the anulus fibrosus predicted by a three-dimensional finite element model and *in situ* morphology, Cell. Mol. Bioeng. 2 (2009) 306–319.
- [47] D. Périé, D. Korda, J.C. latridis, Confined compression experiments on bovine nucleus pulposus and annulus fibrosus: sensitivity of the experiment in the determination of compressive modulus and hydraulic permeability, J. Biomech. 38 (11) (2005) 2164–2171.
- [48] D.T. Pham, J.G. Shapter, J.J. Costi, Tensile behaviour of individual fibre bundles in the human lumbar anulus fibrosus, J. Biomech. 67 (2018) 24–31.
- [49] U. Grömping, Relative importance for linear regression in R: the package relaimpo, J. Stat. Softw. 17 (2007) 1–27.
- [50] F. Heuer, H. Schmidt, H.J. Wilke, The relation between intervertebral disc bulging and annular fiber associated strains for simple and complex loading, J. Biomech. 41 (5) (2008) 1086–1094.
- [51] G.D. O'Connell, E.J. Vresilovic, D.M. Elliott, Human intervertebral disc internal strain in compression: the effect of disc region, loading position, and degeneration, J. Orthop. Res. 29 (4) (2011) 547–555.
- [52] D.L. Skaggs, M. Weidenbaum, J.C. latridis, A. Ratcliffe, V.C. Mow, Regional variation in tensile properties and biochemical composition of the human lumbar anulus fibrosus, Spine 19 (12) (1994) 1310–1319.
- [53] E.R. Acaroglu, J.C. Latridis, L.A. Setton, R.J. Foster, V.C. Mow, M. Weidenbaum, Degeneration and aging affect the tensile behavior of human lumbar anulus fibrosus, Spine 20 (24) (1995) 2690–2701.
- [54] Y. Fujita, N.A. Duncan, J.C. Lotz, Radial tensile properties of the lumbar annulus fibrosus are site and degeneration dependent, J. Orthop. Res. 15 (6) (1997) 814–819
- [55] D.M. Elliott, L.A. Setton, Anisotropic and inhomogeneous tensile behavior of the human anulus fibrosus: experimental measurement and material model predictions, J. Biomech. Eng. 123 (3) (2001) 256–263.
- [56] G.D. O'Connell, H.L. Guerin, D.M. Elliott, 2009. Theoretical and uniaxial experimental evaluation of human annulus fibrosus degeneration.
- [57] M.A. Adams, T.P. Green, Tensile properties of the annulus fibrosus: I. The contribution of fibre-matrix interactions to tensile stiffness and strength, Eur. Spine J. 2 (1993) 203–208.
- [58] J.M. Cloyd, D.M. Elliott, Elastin content correlates with human disc degeneration in the anulus fibrosus and nucleus pulposus, Spine 32 (17) (2007) 1826–1831
- [59] L.J. Smith, N.L. Fazzalari, The elastic fibre network of the human lumbar anulus fibrosus: architecture, mechanical function and potential role in the progression of intervertebral disc degeneration, Eur. Spine J. 18 (2009) 439–448
- [60] D. Cyril, A. Giugni, S.S. Bangar, M. Mirzaeipoueinak, D. Shrivastav, M. Sharabi, J.L. Tipper, J. Tavakoli, Elastic fibers in the intervertebral disc: from form to function and toward regeneration, Int. J. Mol. Sci. 23 (16) (2022) 8931.

[61] J.Y. Tseng, A.A. Ghazaryan, W. Lo, Y.F. Chen, V. Hovhannisyan, S.J. Chen, H.Y. Tan, C.Y. Dong, Multiphoton spectral microscopy for imaging and quantification of tissue glycation, Biomed. Opt. Express 2 (2) (2011) 218–230.

Acta Biomaterialia xxx (xxxx) xxx

- [62] S. Ebara, J.C. Iatridis, L.A. Setton, R.J. Foster, V.C. Mow, M. Weidenbaum, Tensile properties of nondegenerate human lumbar anulus fibrosus, Spine 21 (4) (1996) 452–461.
- [63] J.P. Thompson, R.H. Pearce, M.T. Schechter, M.E. Adams, I.K. Tsang, P.B. Bishop, Preliminary evaluation of a scheme for grading the gross morphology of the human intervertebral disc, Spine 15 (5) (1990) 411–415.
- [64] M. Handl, E. Filova, M. Kubala, Z. Lánský, L. Koláčná, J. Vorlíček, T. Trč, M. Pach, E. Amler, Fluorescent advanced glycation end products in the detection of factual stages of cartilage degeneration, Physiol. Res. 56 (2) (2007) 235–242.
- [65] P.P.Y. Lui, Tendinopathy in diabetes mellitus patients—epidemiology, pathogenesis, and management, Scand. J. Med. Sci. Sports 27 (8) (2017) 776–787.
 [66] R.R. de Oliveira, K.D.S. de Lira, P.V. de Castro Silveira, M.P.G. Coutinho,
- [66] R.R. de Oliveira, K.D.S. de Lira, P.V. de Castro Silveira, M.P.G. Coutinho, M.N. Medeiros, M.F.H.B.I. Teixeira, S.R.A. de Moraes, Mechanical properties of achilles tendon in rats induced to experimental diabetes, Ann. Biomed. Eng. 39 (2011) 1528–1534.
- [67] A.J. Fox, A. Bedi, X.H. Deng, L. Ying, P.E. Harris, R.F. Warren, S.A. Rodeo, Diabetes mellitus alters the mechanical properties of the native tendon in an experimental rat model, J. Orthop. Res. 29 (6) (2011) 880–885.
- [68] M.Y. Avila, J.L. Navia, Effect of genipin collagen crosslinking on porcine corneas, J. Cataract Refract. Surg. 36 (4) (2010) 659–664.
- [69] Y. Li, G. Fessel, M. Georgiadis, J.G. Snedeker, Advanced glycation end-products diminish tendon collagen fiber sliding, Matrix Biol. 32 (3-4) (2013) 169–177.
- [70] A. Gautieri, F.S. Passini, U. Silván, M. Guizar-Sicairos, G. Carimati, P. Volpi, M. Moretti, H. Schoenhuber, A. Redaelli, M. Berli, J.G. Snedeker, Advanced glycation end-products: mechanics of aged collagen from molecule to tissue, Matrix Biol. 59 (2017) 95–108.
- [71] G.K. Reddy, L. Stehno-Bittel, C.S. Enwemeka, Glycation-induced matrix stability in the rabbit achilles tendon, Arch. Biochem. Biophys. 399 (2) (2002) 174–180.
- [72] R.B. Svensson, S.T. Smith, P.J. Moyer, S.P. Magnusson, Effects of maturation and advanced glycation on tensile mechanics of collagen fibrils from rat tail and Achilles tendons, Acta Biomater. 70 (2018) 270–280.
- [73] M.E. McGann, C.M. Bonitsky, M.L. Jackson, T.C. Ovaert, S.B. Trippel, D.R. Wagner, Genipin crosslinking of cartilage enhances resistance to biochemical degradation and mechanical wear, J. Orthop. Res. 33 (11) (2015) 1571–1579.
- [74] T. Yoshida, J.S. Park, K. Yokosuka, K. Jimbo, K. Yamada, K. Sato, M. Takeuchi, S.I. Yamagishi, K. Nagata, Up-regulation in receptor for advanced glycation end-products in inflammatory circumstances in bovine coccygeal intervertebral disc specimens in vitro, Spine 34 (15) (2009) 1544–1548.
- [75] Y. Hu, Z. Shao, X. Cai, Y. Liu, M. Shen, Y. Yao, T. Yuan, W. Wang, F. Ding, L. Xiong, Mitochondrial pathway is involved in advanced glycation end products-induced apoptosis of rabbit annulus fibrosus cells, Spine 44 (10) (2019) E585.
- [76] R.C. Hoy, D.N. D'Erminio, D. Krishnamoorthy, D.M. Natelson, D.M. Laudier, S. Il-lien-Jünger, J.C. latridis, Advanced glycation end products cause RAGE-dependent annulus fibrosus collagen disruption and loss identified using in situ second harmonic generation imaging in mice intervertebral disk in vivo and in organ culture models, JOR Spine 3 (4) (2020) e1126.
- [77] S. Illien-Junger, F. Grosjean, D.M. Laudier, H. Vlassara, G.E. Striker, J.C. Iatridis, Combined anti-inflammatory and anti-AGE drug treatments have a protective effect on intervertebral discs in mice with diabetes, PLoS ONE 8 (5) (2013) e64302.
- [78] G. Fessel, Y. Li, V. Diederich, M. Guizar-Sicairos, P. Schneider, D.R. Sell, V.M. Monnier, J.G. Snedeker, Advanced glycation end-products reduce collagen molecular sliding to affect collagen fibril damage mechanisms but not stiffness, PLoS ONE 9 (11) (2014) e110948.
- [79] J.J. Costi, E.H. Ledet, G.D. O'Connell, Spine biomechanical testing methodologies: the controversy of consensus vs scientific evidence, JOR Spine 4 (1) (2021) e1138.
- [80] F. Rannou, P. Richette, M. Benallaoua, M. François, V. Genries, C. Korwin-Zmijowska, M. Revel, M. Corvol, S. Poiraudeau, Cyclic tensile stretch modulates proteoglycan production by intervertebral disc annulus fibrosus cells through production of nitrite oxide, J. Cell. Biochem. 90 (1) (2003) 148–157.
- [81] R. Gawri, D.H. Rosenzweig, E. Krock, J.A. Ouellet, L.S. Stone, T.M. Quinn, L. Haglund, High mechanical strain of primary intervertebral disc cells promotes secretion of inflammatory factors associated with disc degeneration and pain, Arthritis Res. Ther. 16 (1) (2014) 1-14.
- [82] M.E. Dombrowski, A.S. Olsen, N. Vaudreuil, B.K. Couch, Q. Dong, M. Tucci, J.Y. Lee, N.V. Vo, G. Sowa, Rabbit annulus fibrosus cells express neuropeptide Y, which is influenced by mechanical and inflammatory stress, Neurospine 17 (1) (2020) 69.
- [83] C.S. Yerramalli, A.I. Chou, G.J. Miller, S.B. Nicoll, K.R. Chin, D.M. Elliott, The effect of nucleus pulposus crosslinking and glycosaminoglycan degradation on disc mechanical function, Biomech. Model. Mechanobiol. 6 (2007) 13–20.
- [84] E. Jazini, A.D. Sharan, L.J. Morse, J.P. Dyke, E.A. Aronowitz, L.K. Chen, S.Y. Tang, Alterations in magnetic resonance imaging T2 relaxation times of the ovine intervertebral disc due to non-enzymatic glycation, Spine 37 (4) (2012) E209.
- [85] J.W. Liu, A.C. Abraham, S.Y. Tang, The high-throughput phenotyping of the viscoelastic behavior of whole mouse intervertebral discs using a novel method of dynamic mechanical testing, J. Biomech. 48 (10) (2015) 2189–2194.